Author/s:
Mossayebi, Z;Shabani, S;Easton, CD;Gurr, PA;Simons, R;Qiao, GG

Title:
Amphiphilic Nanoscale Antifog Coatings: Improved Chemical Robustness by Continuous Assembly of Polymers

Date:
2024-10-24

Citation:
Mossayebi, Z., Shabani, S., Easton, C. D., Gurr, P. A., Simons, R. & Qiao, G. G. (2024). Amphiphilic Nanoscale Antifog Coatings: Improved Chemical Robustness by Continuous Assembly of Polymers. Small, 20 (43), https://doi.org/10.1002/smll.202402114.

Persistent Link:
https://hdl.handle.net/11343/351167

RESEARCH ARTICLE

NANO · MICRO small
www.small-journal.com

Amphiphilic Nanoscale Antifog Coatings: Improved Chemical Robustness by Continuous Assembly of Polymers

Zahra Mossayebi, Sadegh Shabani, Christopher D. Easton, Paul A. Gurr, Ranya Simons, and Greg G. Qiao**

Designing effective antifog coatings poses challenges in resisting physical and chemical damage, with persistent susceptibility to decomposition in aggressive environments. As their robustness is dictated by physicochemical structural features, precise control through unique fabrication strategies is crucial. To address this challenge, a novel method for crafting nanoscale antifog films with simultaneous directional growth and cross–linking is presented, utilizing solid-state continuous assembly of polymers via ring-opening metathesis polymerization ($ssCAP_{ROMP}$). A new amphiphilic copolymer (specified as macrocross–linker) is designed by incorporating polydimethylsiloxane, poly(2-(methacryloyloxy)ethyl) trimethylammonium chloride (PMETAC), and polymerizable norbornene (NB) pendant groups, allowing $ssCAP_{ROMP}$ to produce antifog films under ambient conditions. This novel approach results in distinctive surface and molecular characteristics. Adjusting water-absorption and nanoscale assembly parameters produced ultra-thin (≤100 nm) antifog films with enhanced durability, particularly against strong acidic and alkaline environments, surpassing commercial antifog glasses. Thickness loss analysis against external disturbances further validated the stable surface-tethered chemistries introduced through $ssCAP_{ROMP}$, even with the incorporation of minimal content of cross–linkable NB moieties (5 mol%). Additionally, a potential zwitter-wettability mechanism elucidates antifog observations. This work establishes a unique avenue for exploring nanoengineered antifog coatings through facile and robust surface chemistries.

1. Introduction

Fogging poses significant challenges in various applications, from everyday items to medical, aeronautic, automotive, and many more industries.[1] When condensation-induced fog forms on a surface with a temperature at or below the air's dew point, it hinders transparency through scattering light.[2] To address this, passive antifog approaches have gained widespread interest, broadly categorized into two wettability classes: (super)hydrophilic and (super)hydrophobic.[3] (Super)hydrophilic coatings rapidly spread condensed water into a thin film, whereas (super)hydrophobic surfaces repel discrete water droplets, effectively preventing fog formation. However, (super)hydrophilic surfaces are prone to contamination, frost/ice buildup, excessive water condensation, and dissolution/delamination while (super)hydrophobic coatings have limitations in critical droplet size and require surface tilting for effectiveness.[4–6]

Lee et al.[7] introduced a promising alternative by integrating hydrophilic and hydrophobic segments into zwitter-wettable films, also referred to as amphiphilic or hydrophobic yet hygroscopic films.[8] The term "zwitter-wettability" was used to describe the unique wetting behavior of these surfaces, which appear water-repellent but can absorb water molecules while maintaining optical clarity under fogging conditions. These coatings typically display initial water contact angles above 60 ° which decrease over time, indicating faster water vapor diffusion than the nucleation and growth of condensed water droplets.[9] The integration of both hydrophilic and hydrophobic components balances water absorption and repellence. The hydrophobic segments provide structural integrity, while the hydrophilic segments enhance water interaction, crucial for antifogging performance. The selection and proportion of these components are key for imparting unique antifogging properties. Enhanced antifogging performance can be achieved in zwitter-wettable coatings by controlling amphiphilicity and water absorption capacity.[10] An advantage of zwitter-wettable coatings is the ease of removing organic contaminants, owing to the weak retention forces of the hydrophobic component. Unlike

Z. Mossayebi, S. Shabani, P. A. Gurr, G. G. Qiao
Department of Chemical Engineering
The University of Melbourne
Melbourne, Victoria 3010, Australia
E-mail: gregghq@unimelb.edu.au
Z. Mossayebi, C. D. Easton, R. Simons
CSIRO Manufacturing
Melbourne, Victoria 3169, Australia
E-mail: Ranya.Simons@csiro.au

The ORCID identification number(s) for the author(s) of this article can be found under https://doi.org/10.1002/smll.202402114

DOI: 10.1002/smll.202402114

conventional (super)hydrophilic coatings, the hydrophobic component effectively regulates water uptake, restrains excessive swelling, and prevents delamination, wrinkles, and creases during repetitive drying-swelling cycles, ensuring film stability.[4] Due to their numerous advantages, including ease of preparation, scalability, tuneable structure, and high stability under fogging conditions, there is growing interest in zwitter-wettable films.

Recent research, including our work[11] and others,[12] highlights the existence of non-freezable bound water within amphiphilic networks, preventing frost/ice formation. This offers a significant advantage in developing amphiphilic antifog coatings withstanding aggressive temperature conditions, including those that lead to severe surface frosting.[13] Studies on these coatings indicate that utilizing hydrophilic compounds like poly(ethylene glycol) (PEG),[14] along with polyelectrolytes such as poly(acrylic acid) (PAA),[15] poly(2 (dimethylamino)ethyl methacrylate) (PDMAEMA),[16] and polyzwitterions like poly(sulfobetaine methacrylate) (PSBMA),[13,17,18] could synergistically enhance both antifogging and anti-frosting performance. Recent findings by Bai et al.,[19] show that cationic amphiphilic coatings containing poly(2-(methacryloyloxy)-ethyltrimethyl ammonium chloride) (PMETAC) exhibit stronger interactions with water, leading to a higher content of non-freezable water. This opens a unique avenue for exploring cationic amphiphilic coatings effective in both fogging and frosting conditions.

Equally important in designing effective antifogging materials is their durability against physical and chemical damage. Despite efforts to enhance mechanical robustness,[20–23] antifogging coatings remain susceptible to oxidation and decomposition in chemically aggressive environments,[24] posing challenges in industrial and instrumentation applications like protective windows and gauge lenses.[25] Although mixed organic–inorganic hybrid materials have shown improved resistance to acids and alkalis,[26–29] there is a potential risk of inorganic components leaching out upon exposure to such aggressive media, leading to failure.[30] Thus, the challenge remains to design organic antifogging coatings with exceptional chemical stability without compromising performance.

Up to this point, cross–linking has been crucial for enhancing film stability, regardless of the film fabrication techniques. Layer-by-layer (LbL) assembly,[7,10] semi-interpenetrating polymer networks (SIPNs) through grafting approaches,[13,17,19,23] and many more methods have been explored to fabricate amphiphilic cross–linked films. However, these methods often involve additional postmodification steps for cross–linking, like exposure to ultraviolet (UV) light, heat, or solutions containing cross-linkers, leading to challenges such as potential substrate integrity deterioration, incomplete conversion, and lack of control over cross–linking density.[31,32] In contrast, our group developed a catalyst-induced cross-linking (CIC) technique to cross-link films with precise control under mild conditions without requiring heat or UV light.[32] However, CIC, being a solution-based process, introduces potential limitations related to solvent compatibility and film consistency due to diffusion barriers.

To overcome these challenges, a novel film fabrication methodology in the solid-state has been introduced by our group, known as solid-state continuous assembly of polymers (ssCAP).[33] The ssCAP involves a controlled polymerization procedure of ring-opening metathesis polymerization (ROMP), referred to as $ssCAP_{ROMP}$, to continuously form and cross-link polymer networks with nanoscale precision in a bottom-up fashion. This innovative approach has demonstrated several advantages over existing solid-state film formation techniques including simultaneous directional growth and cross–linking, formation of consistent and pinhole-free films, operation under mild reaction conditions, precise control over thickness and cross–linking density, and the ability to tailor properties through a judiciously predesigned macrocross–linker. The innovation of $ssCAP_{ROMP}$ has enabled us to advance the creation of densely cross–linked nanoscale films with unique morphologies for biomedical applications,[34] as well as patterned and 3D-nanoprinted surfaces with potential uses in a myriad of applications.[35,36]

Hence, in this study, we propose a novel approach utilizing $ssCAP_{ROMP}$ to design stable nano-engineered films for antifogging applications. This work highlights several key contributions. First, it extends the application of $ssCAP_{ROMP}$ to antifog surfaces, allowing for precise control of thickness, consistency, and antifogging functionality in surface-confined/cross–linked films at the nanoscale. Second, the study explores the application of amphiphilic macrocross–linkers in $ssCAP_{ROMP}$, a previously unexplored area, and introduces a newly designed antifog cationic/amphiphilic copolymer tailored specifically for this innovative approach. Third, it demonstrates enhanced stability of antifog functionality under chemically aggressive conditions, attributed to the fabrication technique rather than solely the amphiphilic structure. Furthermore, this work involves film formation under ambient conditions due to the notably low glass transition temperature of the designed macrocross–linker and the oxygen tolerance of the Grubbs Generation III catalyst,[37] presenting a significant advantage of our $ssCAP_{ROMP}$ approach compared to other controlled/surface-initiated (SI) polymerizations, which often require oxygen-free environments, elevated temperatures, or light.[38] Finally, the study explores the underlying antifog mechanism of new amphiphilic coatings. The specific combination of amphiphilic materials and controlled molecular and structural features, achievable through the nanoscale assembly process of $ssCAP_{ROMP}$, enables the optimization of antifogging functionality in thin films that sustain even in challenging environments.

2. Results and Discussion

2.1. Synthesis of Macrocross–linker and Nano-Engineered Coatings via $ssCAP_{ROMP}$ Procedure

The $ssCAP_{ROMP}$ process begins with a substrate functionalized with a Grubbs catalyst as an initiating layer. A macrocross–linker containing polymerizable norbornene moieties is subsequently deposited onto the surface, followed by the growth of surface-confined/cross–linked films through the in-situ solid-state ROMP reaction. The adjustment of film thickness for antifogging performance can be readily achieved by modifying the reaction time and incorporating successive multilayers through re-initiation.

To synthesize the amphiphilic macrocross–linker, we first prepared a PDMS-based RAFT macroinitiator following our previous work,[11] which was subsequently copolymerized with

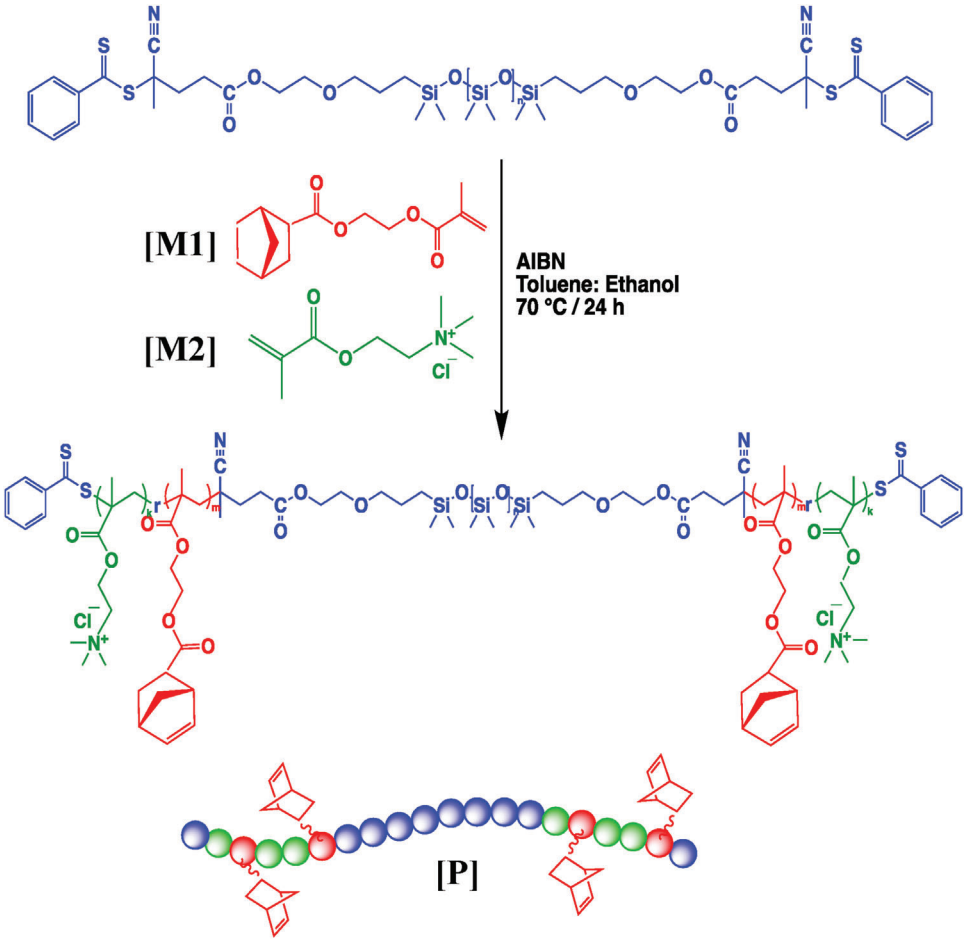

Figure 1. Chemical schematic representing the synthesis of amphiphilic macrocross–linker, denoted as PDMS-b-(P(METAC-r-NBMMA))$_2$.

a preformed norbornene-based monomer (referred to as **M1** in **Figure 1**, Supporting Information Section 1.3.1) and an IL monomer, 2-(methacryloyloxy)ethyl trimethylammonium chloride (METAC) (referred to as **M2**). As shown in Figure 1, this synthesis resulted in the creation of a new cationic/amphiphilic macrocross–linker, which is represented as PDMS-*b*-(P(METAC-*r*-NBMMA))$_2$ and denoted as **P**.

Since antifogging activity is correlated with amphiphilicity,[23,39–43] we systematically adjusted the feed ratios of M1 and M2 monomers to regulate the content of hydrophilic PMETAC segments and hydrophobic norbornene (NB) pendant groups. This resulted in macrocross–linker **P** containing 20 mol% PMETAC and 5 mol% NB pendant groups, as confirmed by ^{1}H NMR (Figure S2 and Table S1, Supporting Information). The selection of macrocross–linker **P** for the subsequent ssCAP$_{ROMP}$ procedure was based on the requirement of an adequate number of NB double bonds for successful CAP$_{ROMP}$, as confirmed in previous studies,[44] while also demonstrating antifog capability through a balance between hydrophilicity and hydrophobicity.

Nano-scale film fabrication via ssCAP$_{ROMP}$ was conducted using a previously established procedure (**Figure 2**). Allyl-modified poly (ethylene imine) (allyl-PEI) was synthesized and characterized, as detailed in Supporting Information Section 1.3.3, for subsequent functionalization of the plasma-treated Si/glass substrates (Figure 2a,b). The allyl-terminated substrates were then exposed to Grubbs Generation III catalyst (see the Supporting Information for pyridine modification/characterization (Section 1.3.4)) to create surface-bound catalysts, forming an initiation layer (Figure 2c). Following either modification step, the surfaces were thoroughly rinsed with appropriate solvents to remove any unattached or physisorbed materials. Although the Grubbs Generation III catalyst allows ROMP reaction in air, CAP$_{ROMP}$ in ambient conditions remains challenging due to catalyst degradation.[45,46] To avoid this, we promptly used the catalyzed surfaces with initiation functional groups and spin-coated a solution of macrocross–linker **P** (50 mg ml^{-1} in $CHCl_3$) onto them. The low glass transition temperature of **P** ($T_g \approx -127$ °C, Supporting Information Figure S5) facilitated the cross–linking and growth of surface-grafted films via CAP$_{ROMP}$ at ambient temperature. After allowing the coatings to stand at room temperature for a predetermined time (1-30 h), they were soaked in a solution of ethyl vinyl ether (2% v/v in DCM), followed by chloroform, to remove any unreacted catalyst and non-cross–linked polymers, respectively. The resulting coatings were then dried for subsequent analysis (Figure 2d). To produce multilayer coatings, all the steps, starting from initiation, are repeated multiple times to the previously formed films, e.g. re-initiation and then

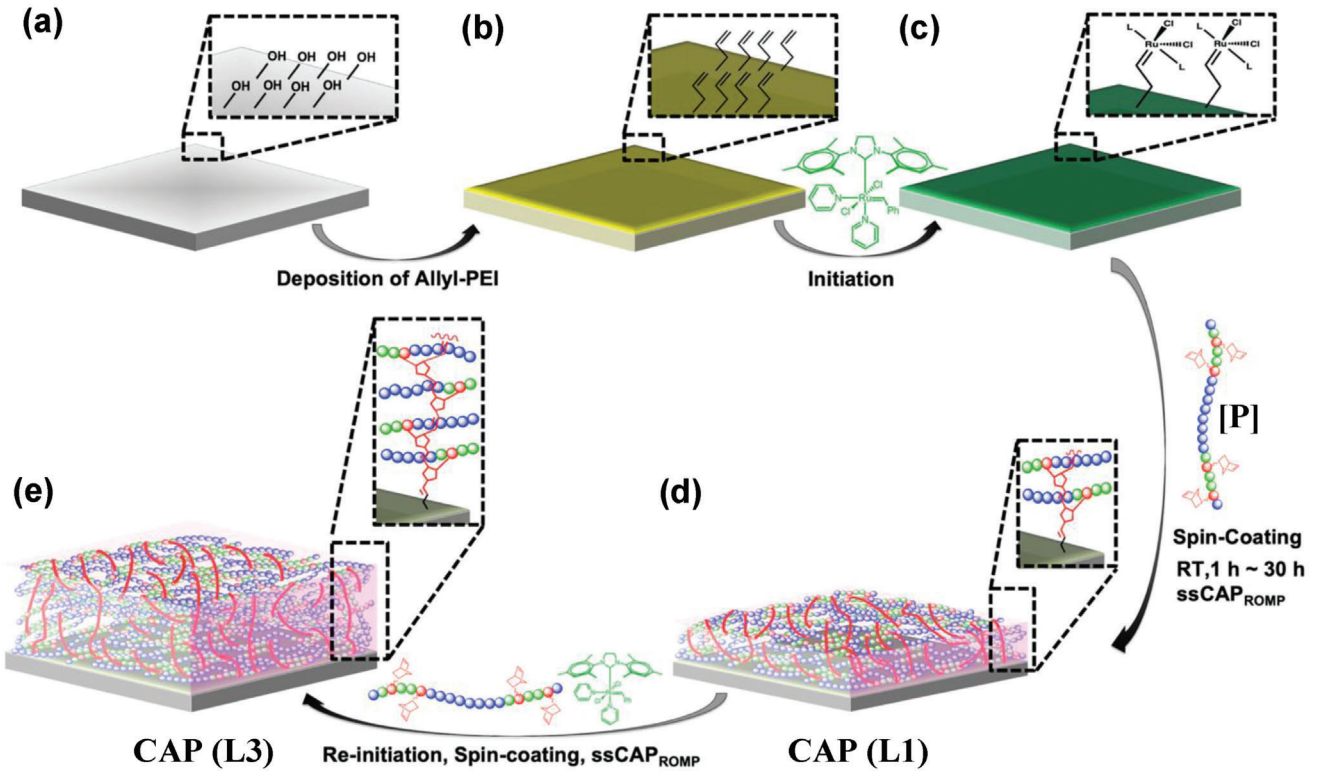

Figure 2. Schematic of solid-state CAP_{ROMP} process for the fabrication of amphiphilic antifogging coatings: a) Plasma-treated substrate/wafer (i.e., W), b) modification with allyl-PEI (i.e., Allyl-terminated W), c) immobilization of initiator (i.e., Catalyzed W), d) macrocross–linker P is applied through spin-coating and after prescribed reaction time, any uncross-linked material is removed by washing and the resulting coatings are dried for further characterization (i.e., CAP (L1)) and, e) to produce multilayer films, all the steps, starting from initiation, are repeated "*n*" times and the ultimate coatings denoted as "CAP (Ln)", where "n" is the number of layers. For example, a triple-layered coating is referred to as "CAP (L3)".

subsequent film formation (Figure 2e). The coatings produced via $ssCAP_{ROMP\ are}$ denoted as "CAP (Ln)", where "n" is the number of layers. Separately, the macrocross–linker **P** was spin-coated onto a cleaned/unmodified substrate, and after drying, it was used as a control coating.

2.2. Growth Kinetics and Surface Characterization of $ssCAP_{ROMP}$ Coatings

The growth kinetics of ssCAP films prepared under different polymerization times in ambient atmosphere were investigated using variable angle spectroscopic ellipsometry (VASE) for thickness measurement. Initially, as depicted in **Figure 3**a, the reaction exhibited a rapid growth rate, which gradually decreased, ultimately reaching a maximum thickness of ≈34 nm after 19 h of polymerization (referred to as L1). A control surface was fabricated by spin-coating macrocross–linker **P** onto the allyl-terminated surface, resulting in no film formation after a 19 h reaction time (Supporting Information Figure S6). This observation indicates that film cross–linking and growth in the L1 thin film were mediated by surface-initiated ROMP. As shown in Figure 3a, prolonged reaction time did not result in thicker films. This limitation can be attributed to the catalyst sites becoming isolated within the highly cross–linked networks of the films, rendering them unavailable to further norbornene pendants of the macrocross–linker due to steric effects.[33] The surface of the cross–linked polymer exhibited a relatively smooth and homogeneous nature, with a root mean square (RMS) roughness below 5 nm acquired by AFM (Figure 3a,b). To further investigate the uniform growth of the CAP layer, we conducted ellipsometric mapping (Figure 3c). The remarkably small deviations in the average thickness of the L1 film ($d = 33.8 \pm 4.5$ nm) across 25 measurement locations within a $0.4 \times 0.4\ cm^2$ surface area suggest that the growth is consistent throughout the formation of L1, indicating uniform coverage of the film across the planar surface. One advantage of $ssCAP_{ROMP}$ chemistry is that the maximum film thickness is not limited to its initial growth (as in Figure 3a). Chain-end fidelity can be maintained through "re-initiation" allowing for sequential polymer chain extension and further film thickness growth. In the L2 film formation, when the L1 film is exposed to Ru catalysts, initiating sites are regenerated through cross-metathesis reactions between the unreacted norbornene pendant groups of the L1 film and the catalyst. This process leads to a surface reactivation able to react with a new layer of macrocross–linker **P**. Consequently, further polymerization and L2 film growth occur. As illustrated in **Figure 4**a, after two rounds of re-initiation (i.e., L3), the film thickness increased to 86.8 ± 4.8 nm, approximately three times thicker than the initial L1 film. Importantly, the multi-layered films remained relatively smooth, demonstrating an overall film roughness of ≈5 nm (Figure 4a,b). Furthermore, thickness mapping of the

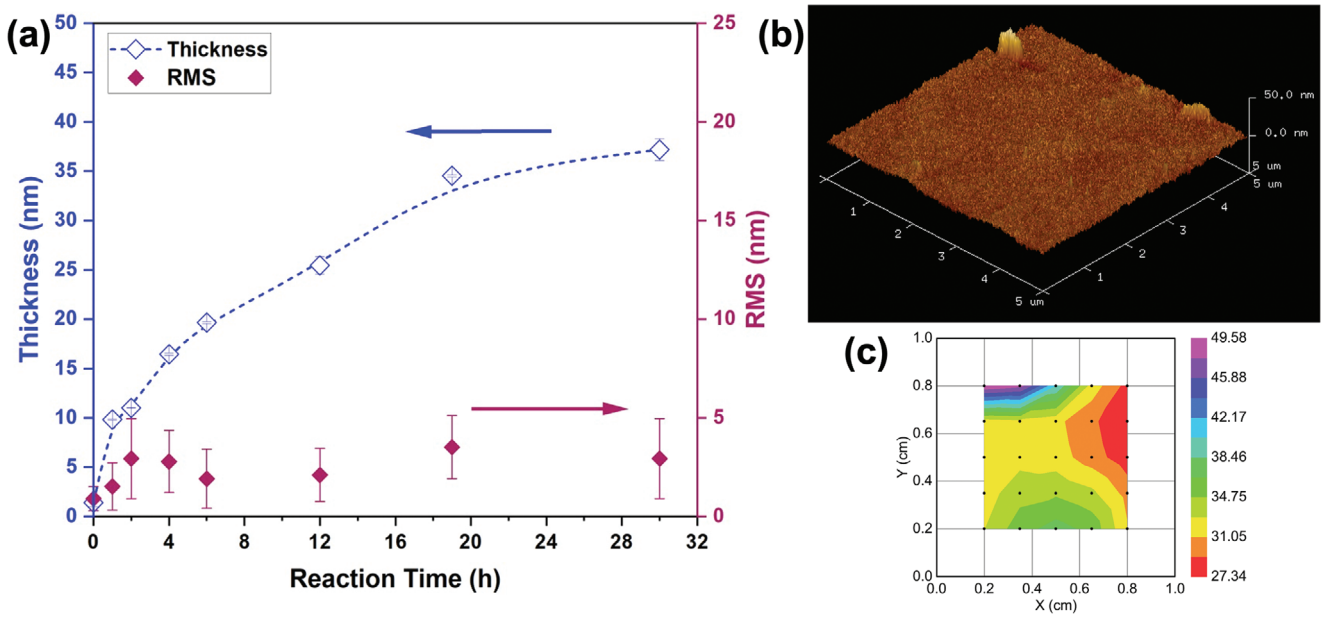

Figure 3. Analysis of ssCAP$_{ROMP}$ films using the P macrocross–linker: a) Kinetics of the film's growth and the corresponding AFM roughness at different reaction times, b) AFM imaging of the film after 19 h ssCAP$_{ROMP}$ polymerization (AFM scale bar is 50 nm), and c) Ellipsometric mapping of the thickness variation across the film formed after 19 h ssCAP$_{ROMP}$ reaction. The image displays thickness at 25 measurement locations within a 0.4 × 0.4 cm^2 surface area (thickness in nm vs position).

L3 film revealed consistent film thickness and uniform film formation as the layers extended (Figure 4c). In contrast, the control spin-coated film displayed significant thickness variations, showing a standard deviation of ≈38% (Supporting Information Figure S7). This highlights the even growth achieved in films produced using ssCAP$_{ROMP}$ chemistry, a feat that is not easily attainable with other solid-state surface-initiated polymerization techniques.[33–35]

To confirm surface-confined ROMP polymerization and identify the chemical composition of surfaces at each fabrication step, XPS analysis was performed, as depicted in **Figure 5**. Initially, on the cleaned Si substrate, the C 1s spectrum displayed a negligible amount of residual organic compounds on the surface (5.6 at.%, Supporting Information Table S2), signifying the effectiveness of the cleaning procedure.[47] Following allyl-functionalization, the amount of carbon increased due to the presence of

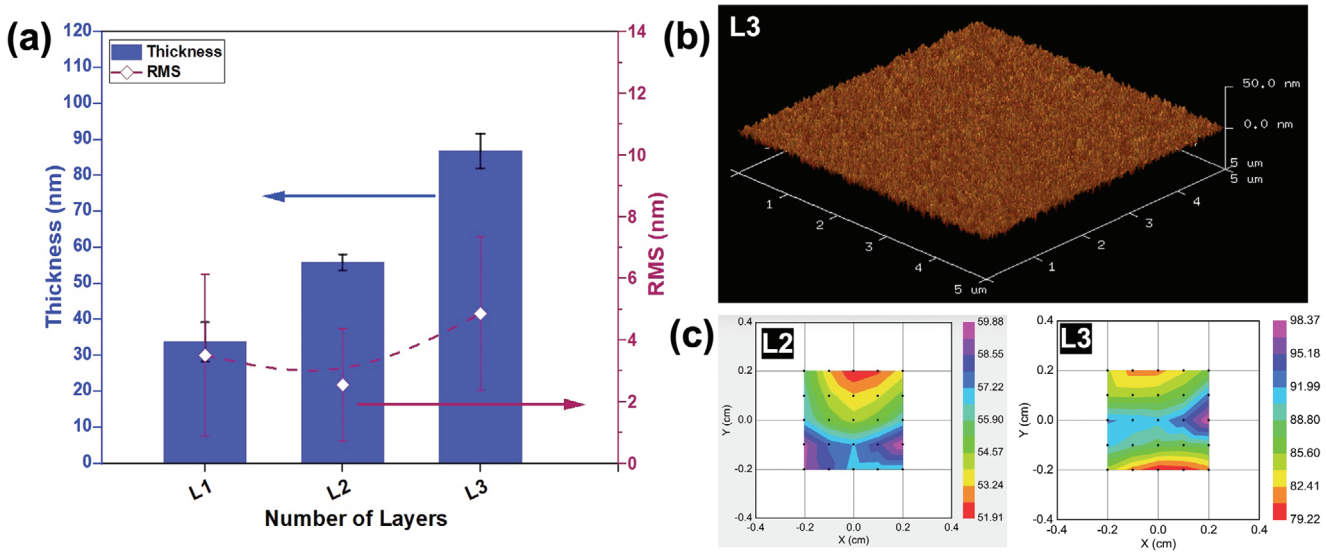

Figure 4. Analysis of multilayered ssCAP$_{ROMP}$ films fabricated via re-initiation procedure: a) Film thicknesses and corresponding AFM roughness of multiple layers, b) AFM imaging of the film after three rounds of re-initiation (i.e., L3), and c) Ellipsometric mapping of the thickness of multilayered L2 and L3 films. The image displays thickness at 25 measurement locations within a 0.4 × 0.4 cm^2 surface area (thickness in nm vs position).

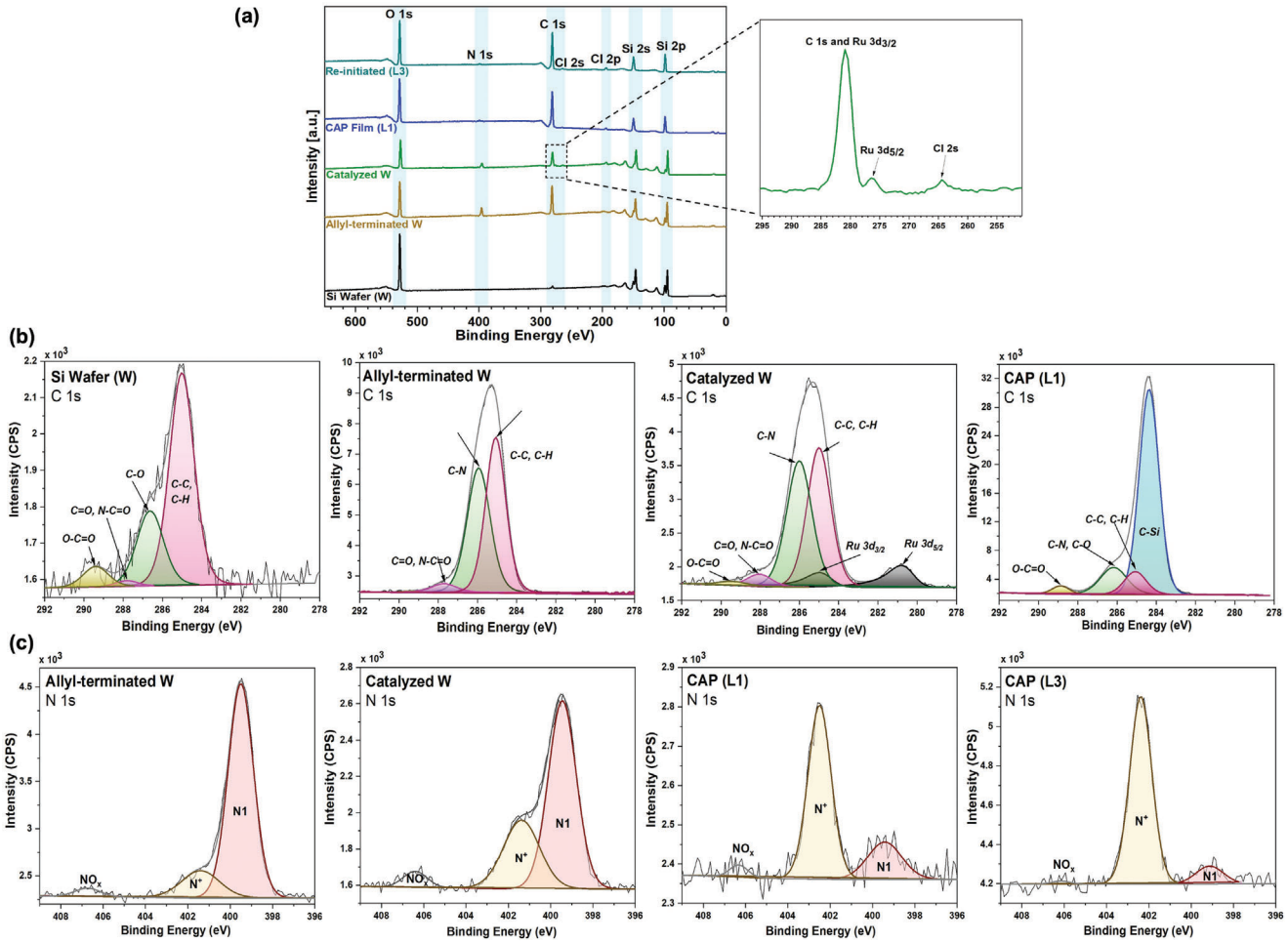

Figure 5. X-ray photoelectron spectroscopy (XPS) data of different surfaces: a) survey and highlights of the ruthenium $3d_{5/2}$ shoulder detected in the sample after initiation with Grubbs catalyst, b) C 1s, and c) N 1s high-resolution spectra of the substrate and different surfaces after progressive steps of the $ssCAP_{ROMP}$ process.

ligands associated with allyl-PEI, primarily C–N (Binding Energy (*BE*)~286 eV) and C–C/C–H (*BE*~285 eV)[48] (36.3 at.%, Supporting Information Table S2). Furthermore, an N 1s peak appeared for the allyl-terminated surface (Figure 5a), with the dominant contribution of component N1 from peak fitting at low *BE* (~399.3 eV), and a high BE peak ≈401.3 eV corresponding to protonated amines (N^+)[49] (Figure 5c). Upon exposure of the allyl-modified surfaces to the Grubbs catalyst solution, the Ru peaks were detected in the C 1s region for the catalyzed surfaces (Figure 5b), confirming that the reaction proceeded.[35] The appearance of shoulders at *BE*~280.9 eV and *BE*~284.9 eV corresponding to Ru $3d_{5/2}$ and Ru $3d_{3/2}$, respectively, along with the emergence of Cl 2p and Cl 2s peaks in the catalyst survey spectra (Figure 5a and Supporting Information Table S2), indicates that the initiation layer, participating in the $ssCAP_{ROMP}$ reaction, effectively bonded to the substrate. Furthermore, the detection of various chemical states in the C 1s spectra (i.e., C–C/C–H and C–N/C–O), N 1s spectra (i.e., N1 and N^+) (Figure 5c), and Si 2p spectra (Figure S8a, Supporting Information) of the catalyzed surfaces, albeit with lower intensity compared to the allyl-terminated surface, provides compelling evidence that the catalyst-immobilized layer serves as an upper layer, but likely thin enough to detect the underlying layers when analyzed in the ultra-high vacuum chamber of the XP Spectrometer.

Following the formation of a surface-confined film via $ssCAP_{ROMP}$ using macrocross–linker **P**, denoted as "CAP (L1)" (Figure 5a), the total amount of carbon increased in comparison to the underlying layers (54.5 at.% for CAP (L1) versus 25.8 at.% for Catalyzed W, Table S2 Supporting Information), which is dominantly attributed to the C–Si signal (*BE*~284.3 eV) originating from the PDMS component of the film. This observation, along with the analysis of N 1s and Si 2p spectra (Figure 5c and Supporting Information Figure S8a), supports the successful assembly of the film on the surface via $ssCAP_{ROMP}$. Regarding the N 1s spectra, the relative fraction of $N1/N^+$ significantly decreased in the CAP (L1) compared to the previous layers (Figure 5c and Supporting Information Table S2). Since N1 is predominantly associated with allyl-PEI, while N^+ is associated with macrocross–linker **P** in the CAP films, the reduction in the $N1/N^+$ ratio confirms that CAP (L1) acts as a top layer for the allyl-modified surface. Re-initiating CAP (L1) three times to create the multi-layered coating "CAP (L3)" more effectively suppressed

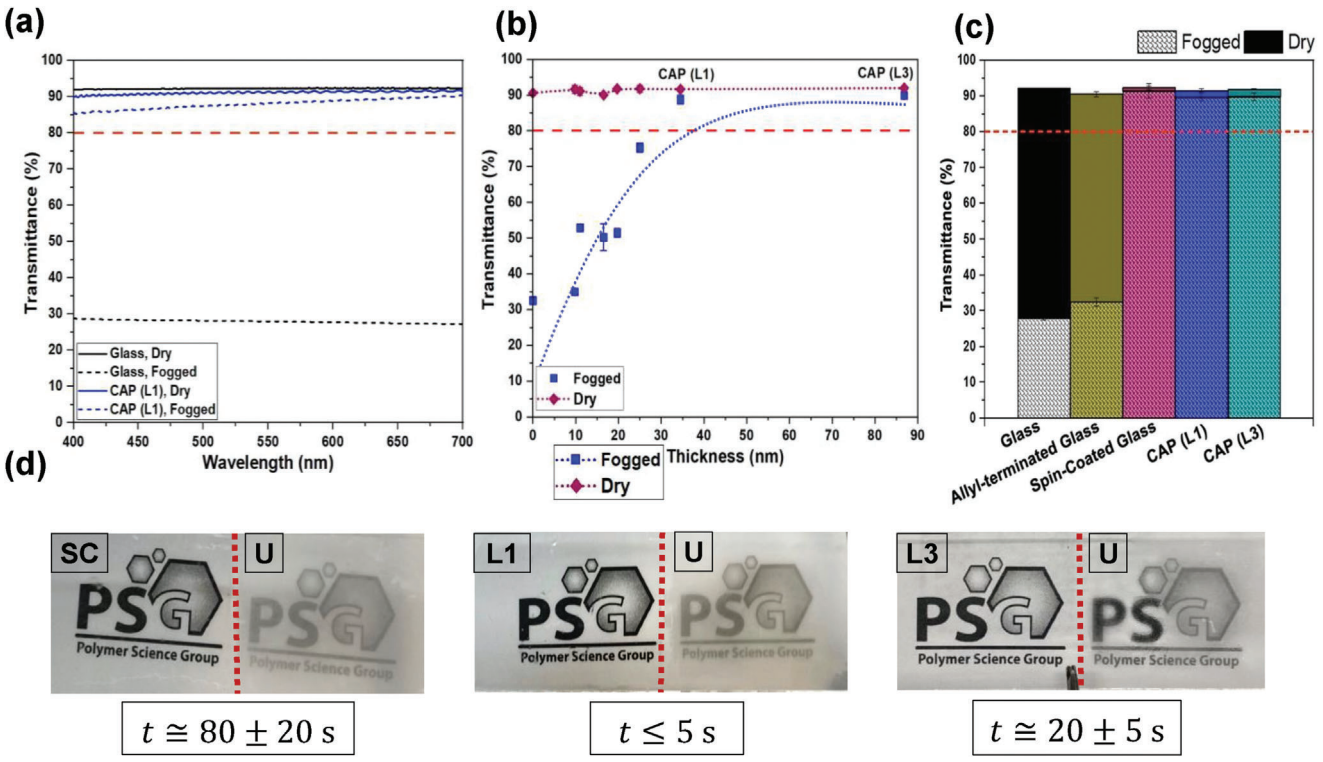

Figure 6. Cold-warm and hot-vapor antifog analysis comparing untreated glass (referred to as U) and ssCAP$_{ROMP}$ coatings: a) Raw data obtained from UV spectrometer within the range of 400-700 nm wavelength as an indication of the light transmission before (dry) and after (fogged) the cold-warm test, b) Thickness-dependent antifogging in coatings fabricated at various ssCAP$_{ROMP}$ reaction times (the average percent light transmission for dry (before) and fogged surfaces during the cold-warm test derived from the raw data in a)), c) Comparison of antifogging performance in CAP coatings (L1 and L3) with control samples, and d) Photographic images of different surfaces were transferred to an ambient environment after exposure to 80 °C hot vapor for a prescribed period of time (hot-vapor test). "SC" is referred to as glass spin-coated with macrocross–linker P.

the N1 peak associated with the underlying allyl-functionalized layer, resulting in a further reduction of the N1/N$^+$ ratio as the film thickness increased (Figure 5c and Supporting Information Table S2).

The thickness and homogeneity of both single-layered and multi-layered CAP coatings were further validated by the attenuation of Si 2p signals from underlying layers due to overlying materials (Supporting Information Figure S8a). Additionally, a comparative analysis of their XPS surveys revealed a thickness sequence of "L1" < "L2" < "L3", as indicated by the background intensity (refer to Supporting Information Figure S8b, see rising background), aligning consistently with ellipsometry results.

2.3. Thickness-Dependent Antifogging Performance of Coatings

We explored the antifogging performance of nano-engineered amphiphilic coatings using both cold-warm and hot-vapor methods. In the cold-warm test, ssCAP$_{ROMP}$ coatings having various thicknesses were placed in a freezer at −20 °C for 30 mins, before being exposed to an ambient environment (≈ 20 °C). The light transmission of the coatings both before (dry) and after (fogged) the cold-warm test was determined using a UV spectrophotometer. **Figure** 6a illustrates a representative example of the raw data, which was then converted to the average percent transmittance within the 400–700 nm wavelength range (Figure 6b,c). For a film to be considered antifogging, its transmittance should not fall below 80% under fogging conditions.[50]

The transmission analysis of coatings thinner than CAP (L1), formed at shorter CAP$_{ROMP}$ reaction times exhibited optical clarity of <80% under fogging conditions (Figure 6b), which is inferior to the antifogging performance of CAP L1. Hence, a minimum thickness of ≈34 nm is necessary for the developed amphiphilic films to showcase their antifogging capabilities. The thicker multi-layered CAP (L3) showed no opacity under the same fogging conditions. As we previously reported[11] and by Bai et al.,[19] condensed water from the surrounding cold atmosphere can be absorbed and molecularly bound to the cationic amphiphilic networks containing PMETAC. In such films, the so-called bound water imparts resistance to fog/frost formation even when exposed to temperatures below the normal freezing point of water. We hypothesize that the improved antifogging functionality with increasing CAP film thickness is likely due to the greater amount of bound water, which prevents water crystallization and the resulting opacity.

As depicted in Figure 6c, the transmitted light intensity of the bare glass control and allyl-terminated glass experienced a substantial decrease, falling below 40%. In contrast, CAP (L1) and CAP (L3) coatings remained fully transparent, exhibiting ≈90% light transmission. This level of transparency is comparable to the thicker spin-coated glass coating.

In addition to the cold-warm test, qualitative hot-vapor tests were conducted by holding the samples 3 cm above an 80 °C hot water bath. The duration for which the samples remained fog-free was recorded, after which they were transferred to an ambient environment and immediately photographed. Half of each glass slide was coated with CAP films, while the other half remained untreated as a control. Upon exposure of CAP (L1) to hot vapor, the control side immediately became opaque due to condensation, while the coated side remained fog-free for ≤5 s (Figure 6d). We observed an extended delay in fog build-up with increasing thickness, maintaining perfect clarity for up to 20 ± 5 s in the multi-layered CAP (L3) (Figure 6d). This antifogging behavior can be attributed to the absorption of water vapor within the hydrophilic PMETAC segments of the CAP films. In contrast, the control experiment on the allyl-terminated glass exhibited a substantial loss of transparency, underscoring the effectiveness of the CAP overlayers. In comparison, glass spin-coated with macrocross–linker **P**, having a thickness of 170.4 ± 65.3 nm, extended the antifogging duration to 80 ± 20 s, albeit with uneven excess condensation and subsequent image distortion, likely due to over-swelling (Figure 6d). Overall, the fabricated CAP coatings demonstrated successful antifogging properties under various conditions, whether involving hot vapor or frost.

We present an innovative platform here for creating ultrathin, surface-confined amphiphilic films with controlled thickness. The nano-scale CAP coatings have the potential to resist the formation of wrinkles and creases in repeated drying-fogging cycles, a challenge primarily associated with thick antifogging films that result in light scattering.[4] The homogeneity of our developed CAP coatings, which remains independent of the film's thickness (as demonstrated in the XPS analysis), combined with balanced amphiphilicity, prevents any local over-swelling of the hydrophilic segments and potential image distortion. We have precisely controlled the degree of cross–linking via ssCAP$_{ROPM}$ to fine-tune the antifogging effect. Increasing the proportion of NB pendants in macrocross–linker **P**, from 5% to 10% results in the formation of a denser network with less water absorption capacity than required for effective antifogging. Conversely, incorporating more hydrophilic groups in macrocross–linker **P** can potentially lead to films that are more effective in withstanding fogging tests.

2.4. Wetting Properties and Zwitter-Wettability of ssCAP$_{ROMP}$ Coatings

The time-dependent changes in the contact angle, surface area (S), and volume (V) of water droplets on surfaces for 350 s were measured to understand their antifogging mechanism. As depicted in **Figure 7a**, the contact angle on the control bare glass remained nearly constant over time, demonstrating negligible drop due to water evaporation. In the amphiphilic CAP films (L1 and L3), the water contact angle decreased linearly over time, with a more rapid decrease observed for CAP (L3), reducing from 65 ° to 35 °. This suggests that the decline in the contact angle on the CAP films (L1 and L3) is not solely attributed to water evaporation; absorption also plays a significant role. For the spin-coated surface (d = 170.4 ± 65.3 nm), we initially observed a sharp decline (≈ 62 °in 30 s), which then leveled off to two linear decreases with a slope similar to that of bare glass at the end. This transition from hydrophobicity to superhydrophilicity is attributed to surface reconstruction associated with the reorientation of hydrophilic PMETAC segments to the surface in response to the water droplet (Figure 7c), a well-accepted phenomenon in amphiphilic systems.[51–54]

Another important observation is that the initial water contact angle of CAP films (L1 and L3) decreased from 82 ± 5 ° to 65 ± 2.5 °, compared to the spin-coated glass. This enhanced initial contact angle in the spin-coated sample is due to the non-cross–linked and flexible surface enriched in hydrophobic and soft moieties of PDMS, as confirmed by XPS analysis. In the XPS survey spectra of the spin-coated film (Supporting Information Figure S9), no discernible peaks associated with N 1s and Cl 2p were detected. This absence of peaks suggests that the low surface energy hydrophobic PDMS groups are oriented toward the surface. Consequently, based on XPS elemental quantification (Supporting Information Table S2), the relative fraction of Si2/C (Si2 assigned to siloxane groups) significantly increased in the spin-coated film compared to the CAP films (L1 and L3), indicating the enrichment of hydrophobic siloxane on the surface of the spin-coated film and thus a higher initial water contact angle. Increased water contact angle due to high surface roughness, as reported by others,[55] was assumed to be negligible since all surfaces showed a similar range of surface roughness (≈ 5 nm) by AFM analysis.

We further investigated the antifogging mechanism by monitoring changes in the surface area of the droplet (S), represented as $\frac{\Delta S}{S_0}$, where S_0 is the surface area at time zero, and $\Delta S = S - S_0$ (Figure S10, Supporting Information). According to the surface area of the droplet on CAP coatings (L1 and L3) over time, it is indicated that wetting-induced surface deformation did not occur due to their robust and cross–linked networks, meaning that the reduction in water contact angle is mostly attributed to water diffusion. In contrast, the spin-coated glass exhibited a significant increase in S (almost triple of S_0) as the droplet quickly spread due to strong water interactions and potential dissolution (Figure S10, Supporting Information), aligning with time-dependent water contact angle results. Similarly, in previous studies,[7] films with less cross–linking degree exhibited noticeable deformation, whereas highly cross–linked systems remained unaffected by this behavior.

To assess water absorption capacity, we tracked the changes in droplet volume on surfaces, represented as $\frac{\Delta V}{V_0}$, where V_0 is the volume at time zero, and $\Delta V = V - V_0$ (Figure 7b). For CAP coatings (L1 and L3), nearly half of the droplets penetrated the surface, with a slightly faster rate in the thicker film (L3). This indicates that water diffusion into CAP films outpaced nucleation and growth on the surface, confirming their zwitter-wettability. The greater water-absorbing capability of L3, correlated with its increased thickness, is closely linked to its antifogging performance, particularly against hot vapor. This implies that water absorption is the dominant antifog mechanism in the CAP films (Figure 7d), whereas the combined swelling and film-wise condensation mechanism in the spin-coated glass compromise its stability.

To further prove the zwitter-wettability of CAP coatings, we conducted water uptake (swelling) tests using the AFM scratch technique to measure thickness changes of CAP (L3) film after 24 h of water immersion. This coating exhibited a 54% increase

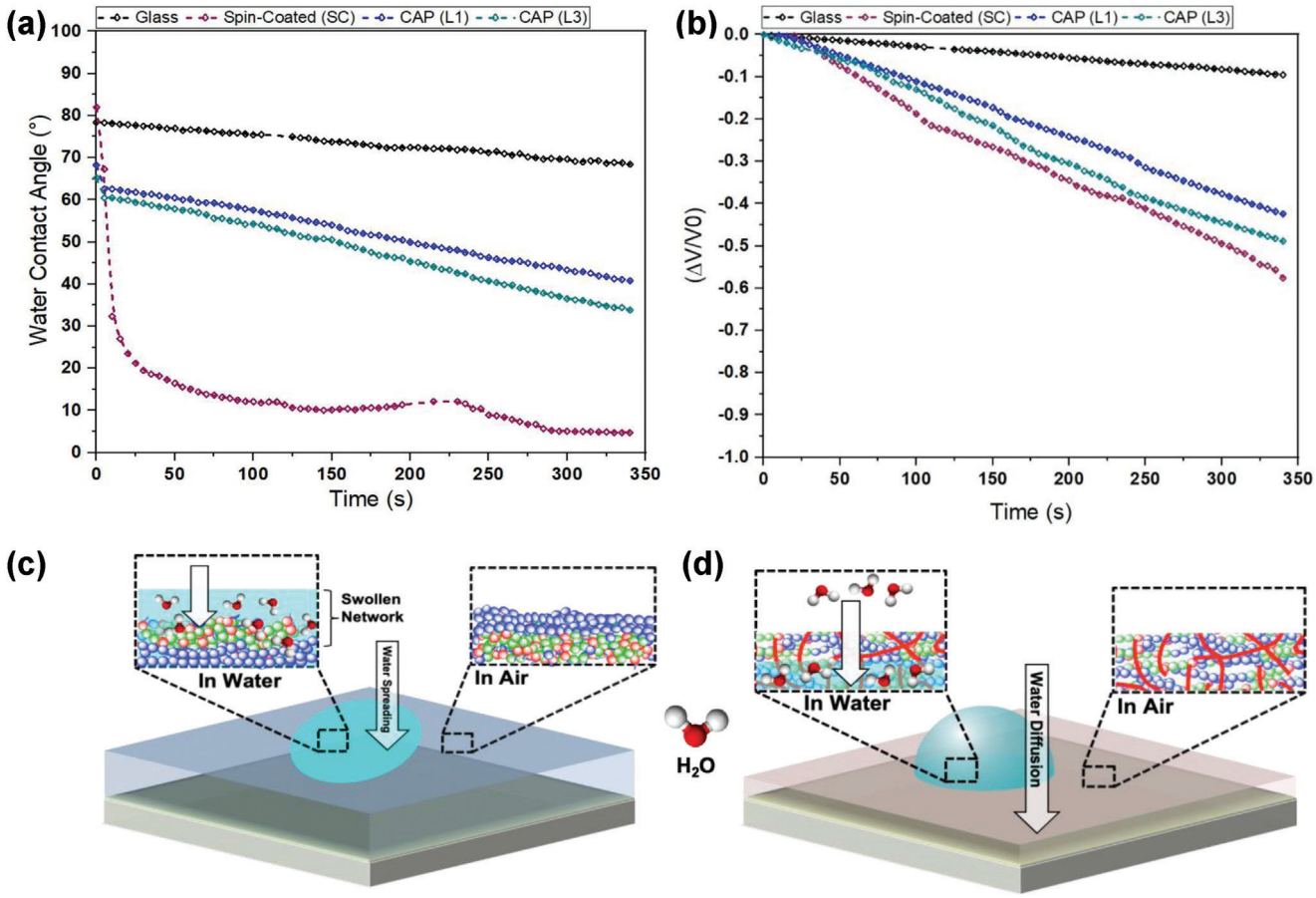

Figure 7. Time-dependent a) water contact angle, and b) volume, over 350 s for the control glass and spin-coated samples as well as single-layer (L1) and multi-layered (L3) ssCAP$_{ROMP}$ films. Schematic representation of the water-surface interactions in c) spin-coated, and d) CAP films.

in thickness (Supporting Information Figure S11), confirming zwitter-wettability behavior.

2.5. Chemical Stability of Antifogging Performance

The susceptibility of antifogging coatings to chemical degradation poses a significant challenge in various industrial applications. To assess the efficacy of our covalently cross–linked films, produced through ssCAP$_{ROMP}$, we conducted anti-fogging performance tests after immersing them in aqueous solutions under various *pH* conditions. These stability tests consisted of an initial fogging experiment, soaking in either acidic (*pH* 1.5), neutral (*pH* 7), or basic (*pH* 13.5) solutions, followed by drying and another fogging test. Acidic and alkaline solutions were prepared using 0.1 M hydrochloric acid and sodium hydroxide, respectively, with deionized water serving as the neutral solution. The coated substrates were immersed in their respective solutions (5 ml per 1 cm^2 of coating) for 1 and 24 h and then underwent assessments through both cold-warm and hot-vapor fogging tests. These results were compared to those of a control spin-coated (SC) glass and commercially available antifog lens.

As shown in Figure S12 (Supporting Information), a 3M commercial lens failed to maintain antifogging performance after 1 hour of soaking in a basic solution, with light transmission dropping to ≈60% following the cold-warm test. Similar observations were made for the spin-coated (SC) glass, not only after 1 hour of soaking in basic solution but also in acidic media. In contrast, CAP coatings (L1 and L3) maintained light transmission (≥80%) under fogging conditions after soaking at each of the three *pH* levels. When extending the soaking time to 24 h (**Figure 8a**), the commercial lens only maintained stability under neutral conditions, while the spin-coated glass proved ineffective under all three conditions. This ineffectiveness can be attributed to the physiosorbed adhesion of these coatings to the substrate, which makes them susceptible to immediate delamination upon exposure to aqueous solutions, limiting their long-term performance. Conversely, CAP coatings (L1 and L3) retained their antifogging performance (light transmission ≥ 80%) even after prolonged exposure to all tested *pH* levels. However, it was observed that the thinner CAP film (L1) was not as transparent as the thicker film (L3) during the cold-warm test, especially after immersion in the strong acidic solution.

We further evaluated the stability of the multi-layered CAP film (L3) and the commercial antifog lens using a hot-vapor test. They were initially subjected to the hot-vapor test, followed by immersion in neutral, acidic, and alkaline solutions, and then another hot-vapor test to detect any potential changes in their fog-free

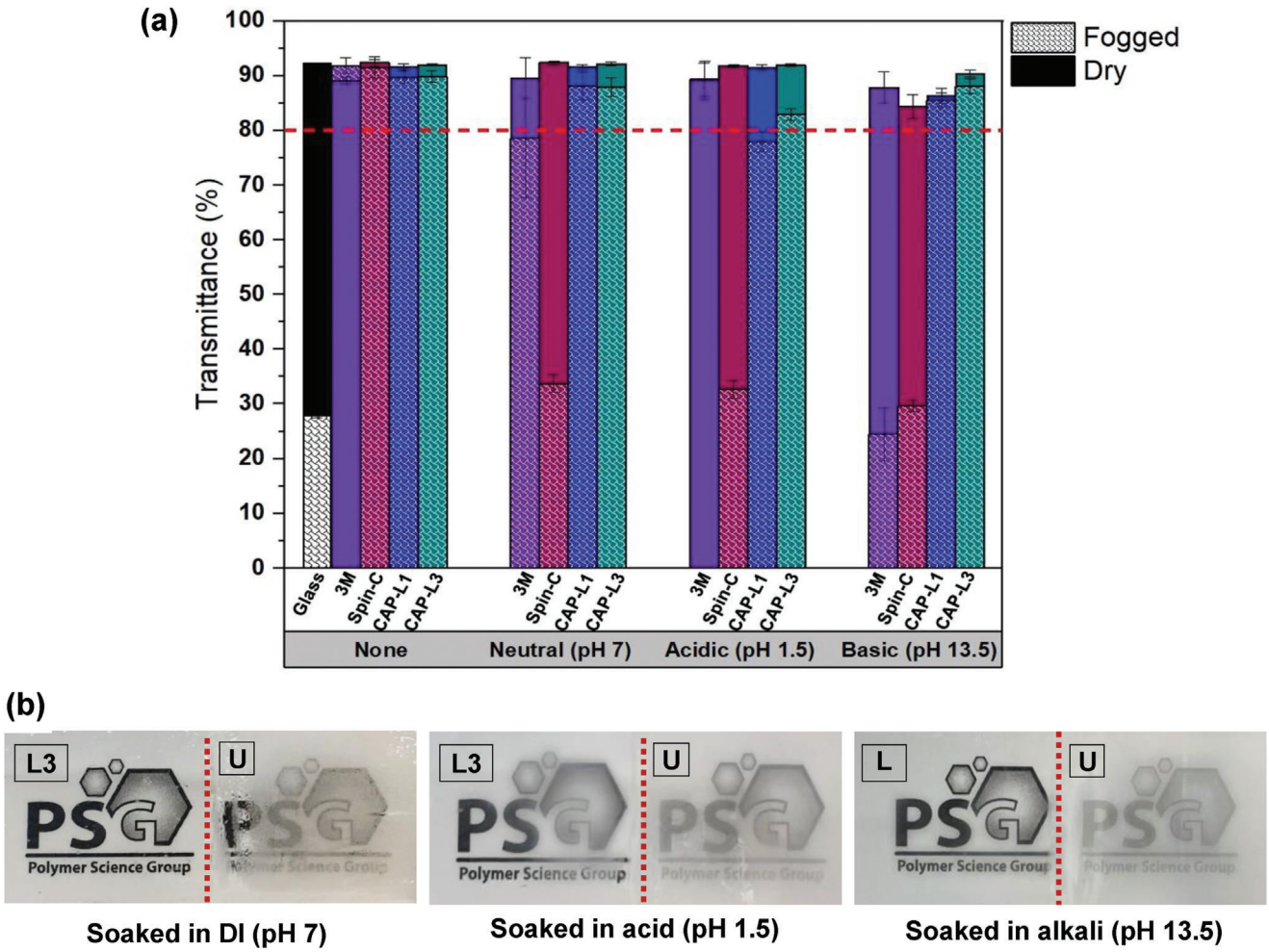

Figure 8. Analysis of chemical robustness of the coatings using both cold-warm and hot-vapor tests. a) Comparison of the light transmission (%) of dry and fogged samples upon initial use as well as following 24 h of soaking in various solutions and then exposing to the cold-warm antifog test. Bare glass, commercial 3M, and spin-coated glass were used as the control samples. b) Photographic images of the multilayered CAP films (L3) were taken after they were soaked for 24 h in various solutions and exposed to hot vapor (80 °C) for 20 s (hot-vapor test). The samples were transferred to an ambient environment after the test to capture the images.

duration before and after immersion. The commercial lens initially resisted vapor condensation, but its antifogging effectiveness was lost after one hour of soaking in various solutions (see Supporting Information Figure S13). In contrast to the commercial lens, which fogged immediately upon exposure to hot vapor, the CAP film (L3) remained fog-free for ≈20 s, nearly the same as before immersion. This coating (L3) was then submerged in each solution (acidic (*pH* 1.5), neutral (*pH* 7), and basic (*pH* 13.5)) for an extended duration of 24 h and again exposed to hot vapor (80 °C) for 20 s. As observed in Figure 8b, there was no loss of optical clarity for these coatings during the hot-vapor test.

In summary, the multi-layered CAP film (L3) outperformed the commercially available antifog glasses in both quantitative light transmission analysis (i.e., cold-warm) and qualitative hot-vapor tests after exposure to neutral, acidic, and alkaline solutions (see Supporting Information, Table S3). This superior performance can be attributed to the strong covalent bonds forming a robust cross–linked network throughout the film. As previously demonstrated,[35] there is no significant morphological variation in the multi-layered CAP film, as the covalent interlayer polynorbornene cross–links securely bound layers together. Consequently, the intimately cross-linked layers did not delaminate or degrade even after multiple processing steps. As reported here, the surface-tethered $ssCAP_{ROMP}$ chemistry proves to be a robust approach in preventing film degradation against various external disturbances, thus ensuring excellent stability of antifogging coatings.

To further substantiate the robust surface chemistry of the ssCAP process, a hydrophobic PDMS-based triblock macrocross–linker was synthesized, containing 10 mol% PNB pendants but lacking PIL segments. Using this macrocross–linker, thin films were formed and tested for chemical stability by measuring the static water contact angle after exposure to acidic, neutral, and basic solutions for 24 h. The results, shown in Figure S14 (Supporting Information), indicated no change in contact angle, demonstrating the enhanced chemical stability of the ssCAP process.

The fabrication of highly stable antifog surfaces, using currently reported techniques, is challenging as surface components

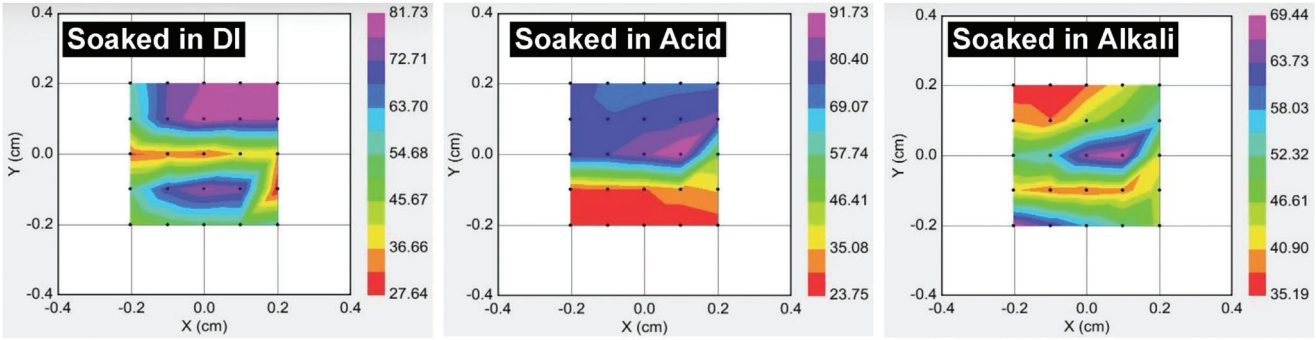

Figure 9. Ellipsometric mapping of the thickness of multilayered CAP films (L3) after soaking for 24 h in various solutions of neutral (pH 7), acidic (pH 1.5), and basic (pH 13.5). The image displays thickness at 25 measurement locations within a 0.4 × 0.4 cm^2 surface area (thickness in nm vs position).

may decompose or leach out under strong acidic and alkaline conditions.[26,28–30,42] Despite not having a mixed organic/inorganic structure, our nanoengineered CAP coating (L3) stands out as one of the most chemically durable organic coatings reported thus far for antifog functionality.

To further explore the stability of the CAP (L3) films, we measured their thicknesses after the various chemical stability tests. As shown in **Figure 9**, while CAP (L3) coating does not exhibit delamination or significant localized defects after exposure to the varying *pH* solutions, a slight reduction in the film thickness still occurs. This film thickness loss can be attributed to possible oxidative cleavage of olefin functionalities within the film network as previously reported.[56,57] However, further investigations will be conducted to propose a detailed mechanism explaining this observation. Overall, the film thickness and consistency remain similar to that of the initial CAP (L3) film, demonstrating the increased robustness of the coatings created using $ssCAP_{ROMP}$ technique.

2.6. Mechanical Durability of Antifogging Coatings

Mechanical durability is another crucial consideration for practical applications of antifogging coatings. Mechanical tests were conducted in accordance with the MIL-C-48497 standard, which is one of the most suitable specifications for optical coatings. A moderate abrasion test was performed to assess whether the films could withstand cleaning and handling in a semi-controlled environment. This test involved rubbing a cheesecloth pad (MIL-CCC-440) across the surface at a constant force (i.e., 26.7 kPa) for a specified number of cycles. To evaluate the adhesion of the films to the substrate, we applied pressure-sensitive tape (3 M Scotch 600) onto the coating surface and then peeled it off at a 180 ° angle. The antifogging performance of the films was compared before and after each mechanical durability test using the cold-warm method. Additionally, we conducted the crosshatch test following a previously established procedure (test method B, ASTM D3359-09$^{\varepsilon 2}$).[11]

Since the multilayered CAP film (L3) demonstrated the best results in terms of fog resistance and chemical robustness, it was selected for the mechanical durability measurements and compared to the **P**, spin-coated onto the glass. As expected, the tape peeling test had no impact on the light transmission of CAP film (L3) during the cold-warm test (Supporting Information Figure S15a, Supporting Information). CAP film (L3) also maintained excellent transparency even after 30 abrasion cycles, with only a slight decrease in average light transmittance under fogging conditions. In contrast, the control spin-coated glass exhibited severe fogging after the abrasion test. As discussed earlier, this is attributed to the physiosorbed nature of the spin-coated film compared to the covalently bonded CAP coating.

Furthermore, we examined the surface of the coatings after the crosshatch test using Field Emission Scanning Electron Microscopy (FESEM) imaging. As shown in Figure S15b (Supporting Information), no noticeable damage was observed along the crosshatched lines of the multilayered CAP (L3) surface, whereas the spin-coated sample was partially delaminated. These observations confirm the mechanical integrity of the surface-confined and cross–linked coating fabricated via $ssCAP_{ROMP}$ procedure.

3. Conclusion

In conclusion, we have introduced a novel approach, solid-state continuous assembly of polymers through ring-opening metathesis polymerization ($ssCAP_{ROMP}$), to create highly stable nano-engineered antifog coatings with simultaneous directional growth and cross–linking. Through a new cationic copolymer design, which combines polydimethylsiloxane (PDMS), hydrophilic poly(2-(methacryloyloxy)ethyltrimethylammonium chloride) (PMETAC), and polynorbornene pendants, thin films were achieved under ambient conditions with controlled thickness and consistency. A minimum film thickness of ≈34 nm was required to resist fog formation through the cold-warm test. In addition, the onset of fog formation through the hot-vapor test was further delayed by up to 20 ± 5 s with the controlled addition of two extra layers, reaching 86.8 ± 4.8 nm. This can be improved by applying additional layers through re-initiation. Notably, this multi-layered coating retained its antifog performance even after prolonged immersion (24 h) in aqueous, acidic, and oxidative environments. This superior stability, which outperformed a commercial antifog lens, results from the robust surface-tethered chemistries introduced through $ssCAP_{ROMP}$, as confirmed by film thickness analysis post-stability tests. Furthermore, the mechanism of antifogging was suggested to

be zwitter-wettability. This study highlights the potential of CAP nanotechnology in enhancing film stability and suggests future research directions for exploring more robust alternatives. Our developed amphiphilic coatings hold great promise for applications requiring robust, controlled, and ultra-thin interfaces with water-absorbing capabilities.

Supporting Information

Supporting Information is available from the Wiley Online Library or from the author.

Acknowledgements

The authors would like to express their gratitude to Thomas G. Pattison for his insights into the ssCAP$_{ROMP}$ procedure. ZM also acknowledges Tom Raeber for his support with AFM analysis. This work was performed in part at the Materials Characterisation and Fabrication Platform (MCFP) at the University of Melbourne and the Melbourne Centre for Nanofabrication (MCN) in the Victorian Node of the Australian National Fabrication Facility (ANFF). ZM was supported by the University of Melbourne Graduate Research Scholarship and the CSIRO-University of Melbourne student agreement.

Open access publishing facilitated by The University of Melbourne, as part of the Wiley - The University of Melbourne agreement via the Council of Australian University Librarians.

Conflict of Interest

The authors declare no conflict of interest.

Data Availability Statement

The data that support the findings of this study are available from the corresponding author upon reasonable request.

Keywords

amphiphilic, antifogging, chemical stability, Continuous Assembly of Polymers, poly(ionic liquids), thin films

Received: March 18, 2024
Revised: June 20, 2024
Published online:

[1] J. Chu, G. Tian, X. Feng, *Nanoscale* **2023**, *15*, 27.
[2] I. R. Durán, G. Laroche, *Prog. Mater. Sci.* **2019**, *99*, 106.
[3] I. R. Durán, G. Laroche, *Adv. Colloid Interface Sci.* **2019**, *263*, 68.
[4] J. Shi, L. Xu, D. Qiu, *Adv. Sci.* **2022**, *9*, 14.
[5] X. Gong, H. Yu, L. Wang, X. Liu, S. Ren, Y. Huang, Z. Huang, *Adv. Colloid Interface Sci.* **2022**, *309*, 102794.
[6] X. Huang, N. S. Zacharia, *J. Appl. Polym. Sci.* **2015**, *132*, 45.
[7] H. Lee, M. L. Alcaraz, M. F. Rubner, R. E. Cohen, *ACS Nano* **2013**, *7*, 2172.
[8] Z. Han, X. Feng, Z. Guo, S. Niu, L. Ren, *Adv. Mater.* **2018**, *30*, 13.
[9] J. Zaho, L. Song, W. Ming, *Adv. Polym. Sci.* **2019**, *284*, 185.
[10] H. Lee, J. B. Gilbert, F. E. Angilè, R. Yang, D. Lee, M. F. Rubner, R. E. Cohen, *ACS Applied Materials and Interfaces* **2015**, *7*, 1004.
[11] Z. Mossayebi, V. F. Jafari, P. A. Gurr, R. Simons, G. G. Qiao, *ACS Applied Materials and Interfaces* **2023**, *15*, 7454.
[12] D. Chen, M. D. Gelenter, M. Hong, R. E. Cohen, G. H. McKinley, *ACS Applied Materials and Interfaces* **2017**, *9*, 4202.
[13] C. Li, X. Li, C. Tao, L. Ren, Y. Zhao, S. Bai, X. Yuan, *ACS Applied Materials and Interfaces* **2017**, *9*, 22959.
[14] J. A. Howarter, J. P. Youngblood, *Macromol. Rapid Commun.* **2008**, *29*, 455.
[15] Y. Wang, T. Li, S. Li, J. Sun, *Chem. Mater.* **2015**, *27*, 8058.
[16] J. Zhao, L. Ma, W. Millians, T. Wu, W. Ming, *ACS Applied Materials and Interfaces* **2016**, *8*, 8737.
[17] C. Tao, S. Bai, X. Li, C. Li, L. Ren, Y. Zhao, X. Yuan, *Prog. Org. Coat.* **2018**, *115*, 56.
[18] Q. Liu, J. Locklin, *ACS Omega* **2018**, *3*, 17743.
[19] S. Bai, X. Li, R. Zhang, C. Li, K. Zhu, P. Sun, Y. Zhao, L. Ren, X. Yuan, *Chem. Eng. J.* **2019**, *357*, 667.
[20] X. Yu, J. Zhao, C. Wu, B. Li, C. Sun, S. Huang, X. Tian, *Materials and Design* **2020**, *194*, 108956.
[21] J. Xiang, X. Liu, Y. Liu, L. Wang, Y. He, L. Luo, G. Yang, X. Zhang, C. Huang, Y. Zhang, *Chem. Eng. Sci.* **2021**, *242*, 116749.
[22] T. Zhang, L. Fang, N. Lin, J. Wang, Y. Wang, T. Wu, P. Song, *Green Chem.* **2019**, *21*, 5405.
[23] X. Gong, H. Yu, L. Wang, J. Hu, L. Wang, C. Li, *Prog. Org. Coat.* **2023**, *179*, 107523.
[24] S. Kim, J. H. Park, *ACS Applied Materials and Interfaces* **2020**, *12*, 42109.
[25] S. Brian (Flextronics Automotive Inc.), US20130001813A1, **2012**.
[26] X. Liu, L. Xu, S. Zhao, H. Hua, Y. Su, X. Yu, J. Wang, G. Li, Y. Zhang, *RSC Adv.* **2023**, *13*, 23409.
[27] P. Varshney, J. Lomga, P. K. Gupta, S. S. Mohapatra, A. Kumar, *Tribol. Int.* **2018**, *119*, 38.
[28] N. Kanovsky, S. Margel, *ACS Omega* **2022**, *7*, 20505.
[29] X. Xu, T. Zhu, W. Zheng, C. Xian, J. Huang, Z. Chen, W. Cai, W. Zhang, Y. Lai, *Chem. Eng. J.* **2023**, *451*, 137879.
[30] Y. Jeon, S. Nagappan, X. H. Li, J. H. Lee, L. Shi, S. Yuan, W. K. Lee, C. S. Ha, *ACS Appl. Mater. Interf.* **2021**, *13*, 6615.
[31] M. Fromel, D. M. Sweeder, S. Jang, T. A. Williams, S. H. Kim, C. W. Pester, *ACS Appl. Polym. Mater.* **2021**, *3*, 5291.
[32] E. Nam, E. H. H. Wong, S. Tan, Q. Fu, A. Blencowe, G. G. Qiao, *Macromol. Mater. Eng.* **2017**, *302*.
[33] E. Nam, J. Kim, S. N. Guntari, H. Seyler, Q. Fu, E. H. H. Wong, A. Blencowe, D. J. Jones, F. Caruso, G. G. Qiao, *Chem. Sci.* **2014**, *5*, 3374.
[34] S. Tan, E. Nam, J. Cui, C. Xu, Q. Fu, J. M. Ren, E. H. H. Wong, K. Ladewig, F. Caruso, A. Blencowe, G. G. Qiao, *Chem. Commun.* **2015**, *51*, 2025.
[35] T. G. Pattison, A. Spanu, A. M. Friz, Q. Fu, R. D. Miller, G. G. Qiao, *ACS Appl. Mater. Interf.* **2020**, *12*, 4041.
[36] T. G. Pattison, S. Wang, R. D. Miller, G. Y Liu, G. G. Qiao, *Nat. Commun.* **2022**, *13*, 1941.
[37] L. Piola, F. Nahra, S. P. Nolan, *Beilstein J. Org. Chem. 11:221* **2015**, *11*, 2038.
[38] J. Yeow, R. Chapman, A. J. Gormley, C. Boyer, *Chem. Soc. Rev.* **2018**, *47*, 4357.
[39] W. Wang, P. Lu, Y. Fan, L. Tian, S. Niu, J. Zhao, L. Ren, *Chem. Eng. J.* **2019**, *378*, 122173.
[40] Z. Liu, P. Tu, Y. Ji, Z. Cai, H. Wu, B. Xu, *Prog. Org. Coat.* **2023**, *177*, 107413.
[41] Z. Ma, Y. Liu, K. Feng, J. Wei, J. Liu, Y. Wu, X. Pei, B. Yu, M. Cai, F. Zhou, *ACS Appl. Mater. Interf.* **2022**, *14*, 18901.
[42] H. Zhong, X. Liu, B. Yu, S. Zhou, *Biomimetics* **2022**, *7*, 162.
[43] J. Yoon, X. Zhang, M. Ryu, W. H. Kim, K. Ihm, J. W. Lee, W. Li, H. Lee, *ACS Appl. Mater. Interf.* **2022**, *14*, 35064.
[44] S. N. Guntari, T. K. Goh, A. Blencowe, E. H. H. Wong, F. Caruso, G. G. Qiao, *Polym. Chem.* **2012**, *4*, 68.

[45] M. B. Dinger, J. C. Mol, *Eur. J. Inorg. Chem.* **2003**, *2003*, 2827.
[46] M. B. Dinger, J. C. Mol, *Organometallics* **2003**, *22*, 1089.
[47] L. Vanzetti, L. Pasquardini, C. Potrich, V. Vaghi, E. Battista, F. Causa, C. Pederzolli, *John Wiley and Sons Ltd* **2016**, *48*, 611.
[48] T. R. Gengenbach, G. H. Major, M. R. Linford, C. D. Easton, *J. Vac. Sci. Technol., A* **2021**, *39*, 1.
[49] A. Adenier, M. M. Chehimi, I. Gallardo, J. Pinson, N. Vilà, *Langmuir* **2004**, *20*, 8243.
[50] I. F. Wahab, A. R. Bushroa, S. Wee Teck, T. T. Azmi, M. Z. Ibrahim, J. W. Lee, *J Mater Res Technol* **2023**, *23*, 687.
[51] J. A. Crowe-Willoughby, J. Genzer, *Adv. Funct. Mater.* **2009**, *19*, 460.
[52] E. Ruckenstein, S. V. Gourisankar, *J. Colloid Interface Sci.* **1986**, *109*, 557.
[53] A. Horinouchi, H. Atarashi, Y. Fujii, K. Tanaka, *Macromolecules* **2012**, *45*, 4638.
[54] Y. Wang, Q. Dong, Y. Wang, H. Wang, G. Li, R. Bai, *Macromol. Rapid Commun.* **2010**, *31*, 1816.
[55] A. B. D. Cassie, S. Baxter, *Trans. Faraday Soc.* **1944**, *40*, 546.
[56] I. A. Fursule, A. Abtahi, C. B. Watkins, K. R. Graham, B. J. Berron, *J. Colloid Interface Sci.* **2018**, *510*, 86.
[57] M. F. Z. Lerum, W. Chen, *Langmuir* **2009**, *25*, 11250.